NASA DEVELOP National Program
California – JPL

Fall 2018

Alaska Ecological Forecasting

Automated Wetland Hydroperiod Mapping Integrating Optical Satellite Imagery and Synthetic Aperture Radar

DEVELOP Technical Report

Final Draft– November 15th, 2018

Annemarie Peacock (Project Lead)
Briant Fabela
Alice Lin
Adam Vaccaro

Bruce Chapman, NASA Jet Propulsion Laboratory, California Institute of Technology (Science Advisor)

1. Abstract

Alaska's wetlands cover approximately one third of the state and provide a multitude of ecosystem services, including nutrient retention, water purification, and provision of habitat for fish, wildlife, and vegetation. The temporal variation in wetland inundation affects these ecosystem functions, and for effective wetland policy and management, it is important to track patterns and changes in inundation. In collaboration with the US Fish and Wildlife Service (USFWS) and Alaska Satellite Facility (ASF) the fall 2018 NASA DEVELOP Alaska Ecological Forecasting team produced an inundation tool to detect and classify inundation extent in Alaska's wetlands from C-band synthetic aperture radar (SAR) data. The team used Earth observation products, including Sentinel-1 C-SAR, Landsat 8 Operational Land Imager (OLI), PlanetScope, and RapidEye satellite imagery, to create the tool's thresholding algorithm and generate land cover classifications for validation. The inundation tool effectively mapped wetland inundation due to SAR imagery's sensitivity to water and reliable data collection on cloudy days. The optical datasets, Landsat 8 OLI and high resolution Planet imagery, were limited by cloud cover and detection of inundation below vegetation and canopy cover but were helpful for visual validations of Sentinel-1 C-SAR classifications. The tool's ability to map wetland inundation can support the development and refinement of National Wetland Inventory (NWI) wetland maps in Alaska and build the capacity of operational federal programs to use SAR.

Keywords

Remote sensing, wetlands, Alaska, synthetic aperture radar, inundation

2. Introduction

2.1 Background Information

Wetlands cover approximately 43%, or 174 million acres, of Alaska's surface area and provide many important ecosystem functions, such as habitat for birds and fish, insulation from permafrost, water filtration, and flood regulation (Hall, Frayer, & Wilen, 1994). Alaska has numerous types of wetlands, including tundra, marshes, bogs, and permafrost areas. The United States Fish and Wildlife Service (USFWS) established the National Wetlands Inventory (NWI) to monitor the extent, characteristics, and change in the nation's wetlands. The NWI works to create a comprehensive inventory of wetland maps and information to inform the public and resource managers as they engage in wetland protection, emergency planning, and habitat conservation projects (United States Fish and Wildlife Service [USFWS], 2018).

The NWI has traditionally employed technicians to manually delineate wetland extent using fine resolution optical imagery and validation from *in situ* data collection (Wilen & Bates, 1995). However, this procedure is time and resource intensive, especially with Alaska's remote landscape, and NWI products are only available for approximately one third of Alaska. This mapping process lacks the capability to capture many conditions below forest canopies (Tiner, 1990) and also limits the capture of temporal and seasonal variations in inundation (hydroperiod) (Brooks, 2000), which determine wetland extent and function (Lang, Kasischke,

Prince, & Pittman, 2008). Additionally, periodic cloud cover over Alaska wetlands and seasonal variations in photoperiod, the period of time each day where the Earth is illuminated, can make the use of optical imagery for wetland classification unreliable.

Previous work has demonstrated the potential for C-band synthetic aperture radar (C-SAR) backscatter data to map wetland inundation extent (Lang et al., 2008; Townsend, 2002). Sentinel-1 C-SAR uses active remote sensing and transmits and receives its own pulses of electromagnetic radiation, allowing for data acquisition independent of daylight or natural surface illumination. Additionally, SAR emits longer wavelengths in the electromagnetic spectrum that can penetrate clouds, which allows for more frequent data collection unconfined by atmospheric conditions (Kasischke, Melack, & Dobson, 1997). SAR technology can also partially penetrate vegetation canopies and resulting in double bounce interactions between water surfaces and vertical plant structures, significantly increasing SAR backscatter intensity in areas of inundated vegetation (Tsyganskaya, Martinis, Marzahn, & Ludwig, 2018). These qualities make SAR a robust source of data for the close monitoring of wetland hydroperiods, and this project aims to generate inundation land cover classifications from Sentinel-1 C-SAR imagery. Land cover classifications of Landsat 8 OLI and higher resolution optical data can be used to cross validate SAR classifications.

This project aims to assist the NWI with their mapping capabilities in Alaska through a collaboration with the Alaska Satellite Facility (ASF) to produce an inundation mapping product for C-SAR data. This product will be calibrated and validated against Landsat 8 Operational Land Imager (OLI) and Planet Labs optical imagery. Our chosen study sites (Figure 1) encompass a variety of wetland types with different characteristics depending on their flooding regimes and vegetation community (eg., emergent, persistent, forested, shrub) (Table A1). This allows for the evaluation of C-SAR efficacy in determining inundation in the presence of vegetation as well as the creation of a more robust product. We used C-SAR and optical imagery from June 2017 to September 2017 to capture inundation extent during non-frozen conditions.

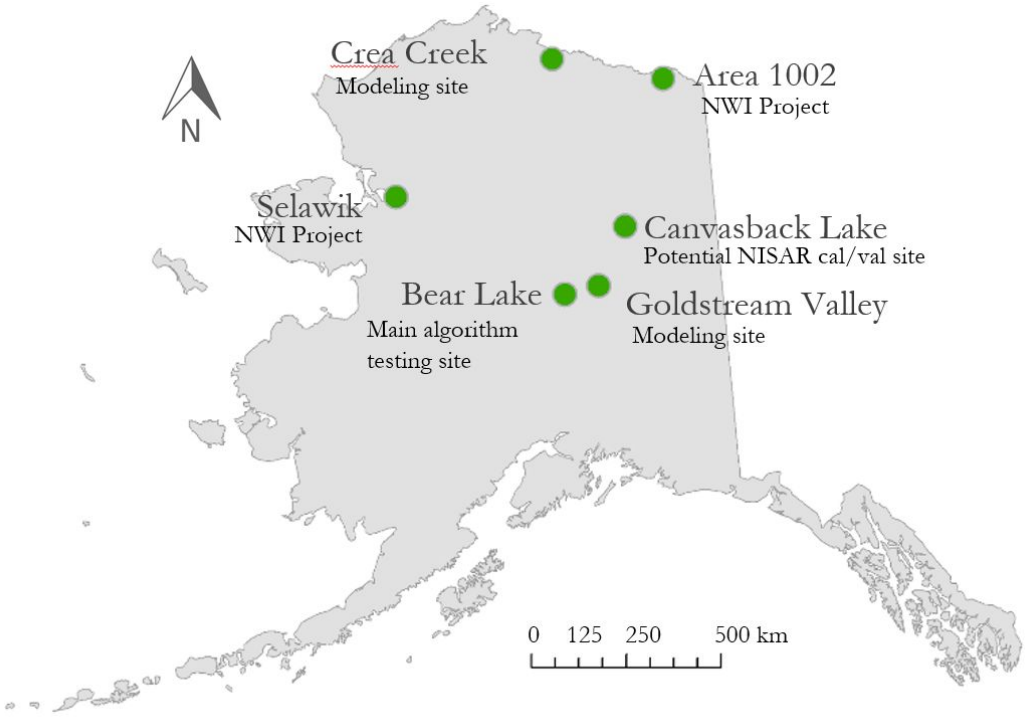

Figure 1. Wetland sites in Alaska used to calibrate and validate inundation algorithm with Sentinel-1 C-SAR, Landsat 8 OLI, and Planet Labs data.

2.2 Project Partners & Objectives

The end user of our product is the USFWS NWI. The NWI has created the Wetlands Mapper, a web based platform that provides detailed digital maps of United States' wetlands for use by resource managers and the public. However, the Wetlands Mapper currently only includes abouts a third of Alaskan wetlands, and the NWI hopes to complete mapping wetland areas in Alaska. The NWI also has a strong interest in enhancing the production of their wetland map products. As of now, their maps are manually created through a combination of visual interpretation of optical imagery and *in situ* validation conducted by field technicians. This process is resource intensive, and the addition of an algorithm for C-SAR inundation classification would enhance their mapping capacity. The NWI will evaluate the inundation algorithm made from C-SAR imagery to assess if they will be beneficial for generating new mapping products and for refining their current wetland maps. Our project will build capacity for the NWI to utilize radar data for wetland mapping and also build on their capacity to automate their mapping process with reliable results.

We collaborated with the ASF, who are the current developers of the Hybrid Pluggable Processing Pipeline (HyP3). HyP3 is a cloud-based C-SAR data archive and processing platform. It provides on-demand processed SAR imagery that has been co-registered and radiometrically corrected. We used this platform to generate wetland inundation maps for the NWI. This platform can facilitate efforts to automate wetland map generation not only in Alaska, but for other wetland areas around the world due to its 'on-demand' nature and global coverage of SAR data. ASF will also benefit from our collaboration as our tool will test the capabilities of their platform when incorporating and executing new algorithms. This will provide valuable feedback for current and future developments of the HyP3 platform.

The project objectives are to implement an algorithm capable of detecting inundation extent in Alaska wetlands from C-SAR data, integrate this tool with ASF's HyP3, and validate inundation products from C-SAR data using optical data. Successful implementation will result in a tool to automatically generate and supply inundation maps to the NWI, which can be used to delineate wetland extent. This will augment the mapping capabilities of the National Wetlands Inventory and add capabilities to ASF's SAR processing.

3. Methodology

3.1 Data Acquisition

We requested 2017 Sentinel-1 C-SAR data with coverage of our study areas from ASF's HyP3 tool data download portal, which provides radiometrically corrected imagery (Hogenson et al., 2016). We downloaded both vertically transmitted vertically received (VV) and vertically transmitted horizontally received (VH) polarized imagery. VV linear polarized waves were of particular interest to our work as they capture the 'double bounce' effect that commonly occurs in inundated vegetation with radar imagery. This effect is a very unambiguous sign of inundated vegetation and helps identify these areas. The available Sentinel-1 scenes in the data portal were first visually analyzed in ASF's Vertex interface to identify the Sentinel-1 paths and frames capturing our study areas in the 'near range' of the sensor. This allows us to utilize imagery with smaller incidence angles which is optimal because it allows for stronger backscatter returns.

We used the USGS Earth Explorer tool to download cloud-free Landsat 8 Operational Land Imager (OLI) Level 2 Surface Reflectance images that corresponded with our Sentinel-1 C-SAR data coverage and

acquisition dates. High-resolution optical imagery included 5 meter resolution RapidEye imagery, and 3 meter resolution PlanetScope imagery. Imagery from these sensors both belong to Planet Labs. The imagery was downloaded from Planet's website using their browsing capability to locate cloud-free images corresponding with Landsat and C-SAR acquisition dates (Table 2).

Table 2
Compilation of dataset information and acquisition

Dataset	Parameters	Metadata	Data Acquisition
Sentinel-1 C-SAR	Backscatter values, surface roughness	Level 1 IW, VV + VH, 5 x 20 m, 12 day composite, June 2017 to September 2017	ASF Vertex/HyP3
Landsat 8 OLI	Surface reflectance	Level 2, 30 m, 8 day composite, June 2017 to September 2017	Earth Explorer
PlanetScope and RapidEye	Surface reflectance	Level 3B, 3 - 5 m, June 2017 to September 2017	Planet Lab

3.2 Data Processing

A number of steps were required to geometrically and radiometrically correct the SAR imagery before analysis. We first verified that the spatial coordinates of the SAR images were encoded in the Universal Transverse Mercator (UTM) projected coordinate system. If they were not, we projected them using a shell script from the Geospatial Data Abstraction Library (GDAL). Next, we converted the SAR images from their native GeoTIFF format into ENVI raster files using another GDAL function. We extracted metadata from the ENVI headers produced during the conversion in order to co-register the images. Once the images had been co-registered, we converted the pixel values into decibels (Equation 1).

(1) brightness (dB) = $10*\log^{10}$(pixel % value)

Having projected and converted the SAR data, we employed two different methods to check if the data were properly calibrated (Chapman et al. 2015). The first method consisted of calculating and plotting VV/ VH band ratios for each scene and visually inspecting for brightness anomalies. For the second method, we calculated the average brightness value for a given scene and plotted it over time (Figure 3).

The optical datasets were manually filtered to imagery with low cloud cover and close correspondence with Sentinel-1 acquisition dates. Landsat 8 OLI images Level 2 Surface Reflectance products have already been calibrated and atmospherically corrected, and the downloaded Planet Labs imagery had already been orthorectified and calibrated for analysis, as well.

3.3 Data Analysis

3.3.1 SAR Classification

The following C-band SAR classification methodology is adapted from a study that used L-band SAR to detect inundation (Chapman et al. 2015). To classify the SAR imagery into open water, inundated vegetation,

and not inundated areas, we performed this procedure on Sentinel-1 C-SAR VV, VH, and VV/VH ratio intensity images. First, we calculated the multi-temporal averages (I_a) from June to September 2017 by averaging data from each SAR acquisition (Figure 2). Compared to individual SAR images, the multi-temporal averages (I_a) have reduced speckle and instead the varying backscatter values highlight environmental changes.

To classify I_a into open water, inundated vegetation, and not inundated, we applied a set of VV, VH, and VV/VH brightness thresholds (Table 4). We determined the brightness thresholds for VV, VH, and VV/VH by manual inspection of backscatter brightness values in the different polarizations and visual comparison with the Planet Labs higher resolution RapidEye and PlanetScope.

These multi-temporal classifications represented the average extent of inundation over the summer of 2017, but did not capture finer temporal variations. In order to quantify the range of inundation states, we compared the backscatter values at individual timesteps to the average inundation state. To account for the speckle noise in individual SAR images, we took a 3x3 pixel moving window average of the scenes and calculated the ratio of these multi-looked images to I_a The range in inundation states also allowed us to determine minimum and maximum inundation area.

3.3.2 Optical Imagery

Landsat 8 OLI images were classified using a workflow based on the Dynamic Surface Water Extent (DSWE) algorithm developed by John W. Jones and Michael J. Starbuck of the US Geological Survey (USGS) (Jones, 2015). This algorithm extracts five land cover classes from Landsat surface reflectance products by determining surface water inundation for each Landsat pixel (Table 3). We wrote a script for Google Earth Engine that obtained specific Landsat 8 OLI scenes and output an initial DSWE classification. The script then masks out areas with snow, cloud shadows, clouds, and steep regions that are unlikely to retain surface water to output the filtered DSWE classification.

Planet Labs' imagery was analysed by applying a Normalized Difference Water Index (NDWI) (Equation 2) to our image layer composites. The main purpose of this index is to highlight and delineate areas of open water. The index also assists in the identification of inundated vegetation and areas of shallow water or high moisture. The Index imagery consists in pixel values ranging from -1 to 1, with negative values indicating dry non-inundated areas, and positive values indicating moist or inundated areas. Another helpful index when identifying partially inundated areas, such as inundated vegetation, was the Normalized Difference Vegetation Index (NDVI) (Equation 3). This index measures vegetation greenness. Areas in the imagery with high values corresponded to closely to densely vegetated areas. Regions in the imagery with coincidently high NDWI values and high NDVI values most often were clear indicators of inundated vegetation. With all of these indexes as well as the original multispectral optical data we performed unsupervised land cover classifications using ENVI which were able to then reliably classify areas of open water, inundated vegetation, and non-inundated areas.

(2) $$\frac{Green-NIR}{Green+NIR}$$

(3) $$\frac{NIR-Red}{NIR+Red}$$

3.3.3 Accuracy Assessments

In the absence of available ground truth data, we instead compared single-date SAR classifications with Landsat 8 DSWE outputs. First, we reclassified both the SAR and Landsat DSWE into binary classifications of inundated and not inundated to facilitate comparison. For the binary reclassification, areas identified in the SAR classifications as inundated vegetation and open water were combined into one inundated class. DSWE was reclassified based on Table 3. To compare the two classifications, SAR and DSWE were both resampled to a resolution of 90 meters. With DSWE and SAR at the same spatial resolution, we calculated a confusion matrix, setting DSWE as the ground truth image.

Table 3

DSWE classes and corresponding reclassified categories

DSWE Category	**Reclassified Category (Binary)**
Not water	Not inundated
High confidence water	Inundated
Moderate confidence water	Inundated
Potential wetland	Inundated
Low confidence water or wetland	Not inundated

4. Results & Discussion

The classification of SAR's multi-temporal averages showed each site's typical inundation extent, and the VV, VH, and VV/ VH polarization images helped distinguish between land cover classes. For the Bear Lake site, open water and inundated vegetation appear darker in the VH image. In the VV image, inundated vegetation is brighter with higher backscatter values, and the smoother open water surfaces are darker with lower backscatter (Figure 2). The differences in backscatter values between inundated vegetation in the VV and VH polarizations are highlighted in the VV/VH ratio, as the inundated vegetation areas appear even brighter in the ratio image (Figure 2). We used these differences in brightness in conjunction with visual comparison of Landsat 8 and Planet Labs imagery to set threshold ranges (Table 4). These threshold values are specific to Bear Lake. For the additional study sites, although inundated vegetation generally appeared darker in VH and brighter VV, the different polarization images must be still manually inspected for specific threshold ranges.

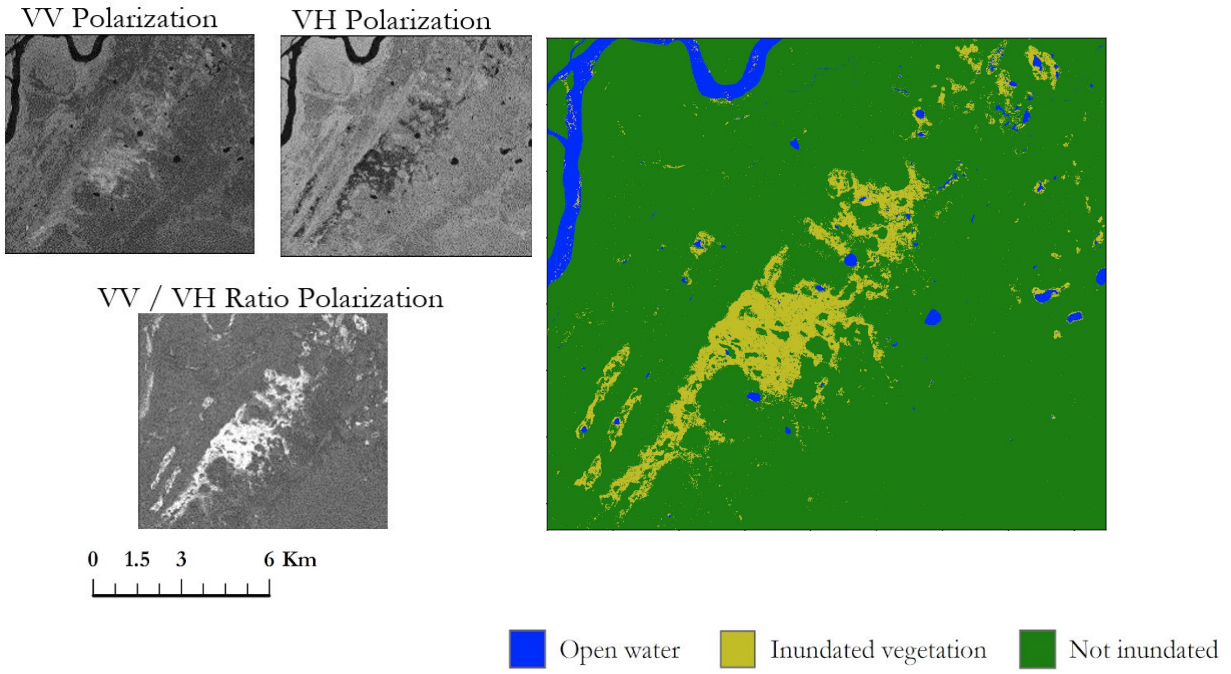

Figure 2. VV, VH, and VV/VH polarizations averages from June 12 2017 - September 28, 2017 on Bear Lake, Alaska. Right multi-temporal average classified from left's VV, VH, and VV/VH brightness thresholds.

Table 4

Brightness threshold values for Bear Lake.

BEAR LAKE	Open Water	Inundated	Not Inundated
VV Low	0	0.1	0.15
VV High	0.2	0.63	0.4
VH Low	0	0	0.15
VH High	0.063	0.33	0.3
VV/VH Low	0	3	0
VV/VH High	10	50	10

Minimum and maximum extent show the fluctuations in inundation at Bear Lake during the summer of 2017 (Figure 3). Minimum inundation shows only the areas that were inundated for all individual SAR acquisitions, and maximum inundation shows all pixels at Bear Lake that were inundated at any time during the acquisition period.

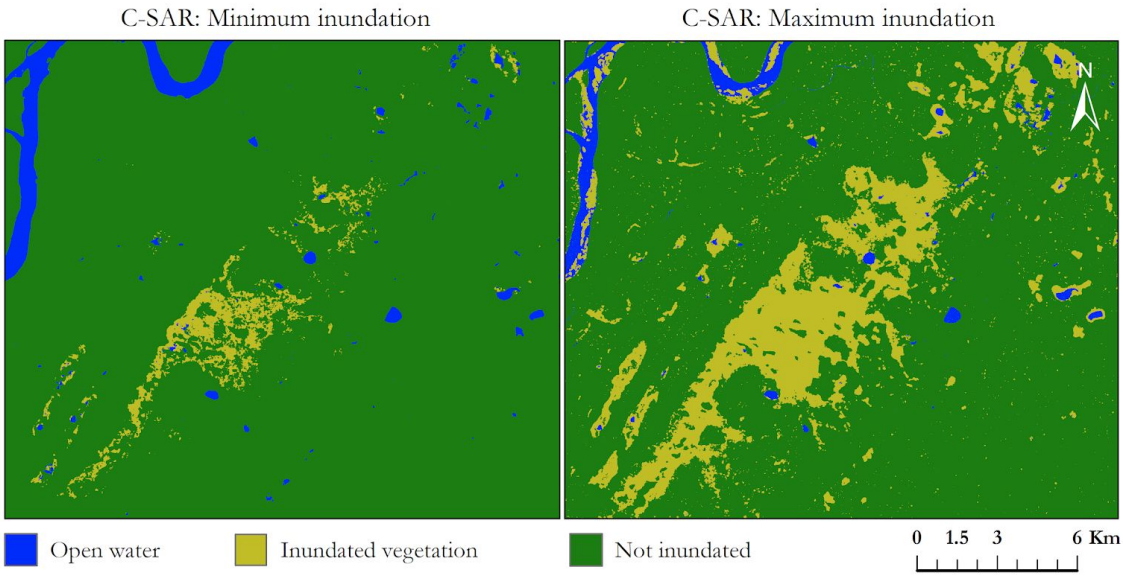

Figure 3. Minimum and maximum inundation extent derived from C-SAR data between June 12 2017 - September 28, 2017 on Bear Lake, Alaska.

Single-date classifications capture smaller temporal changes in inundation and can be used to compare against Landsat DSWE (Figure 4). Comparing the two dataset classifications on similar dates eliminates temporal inundation fluctuations as a source discrepancy in the classifications. Looking at Figure 4, slight differences in the classifications are apparent. Compared to SAR, Landsat DSWE generally included less areas as inundated vegetation but classified more areas as open water (Figure 4).

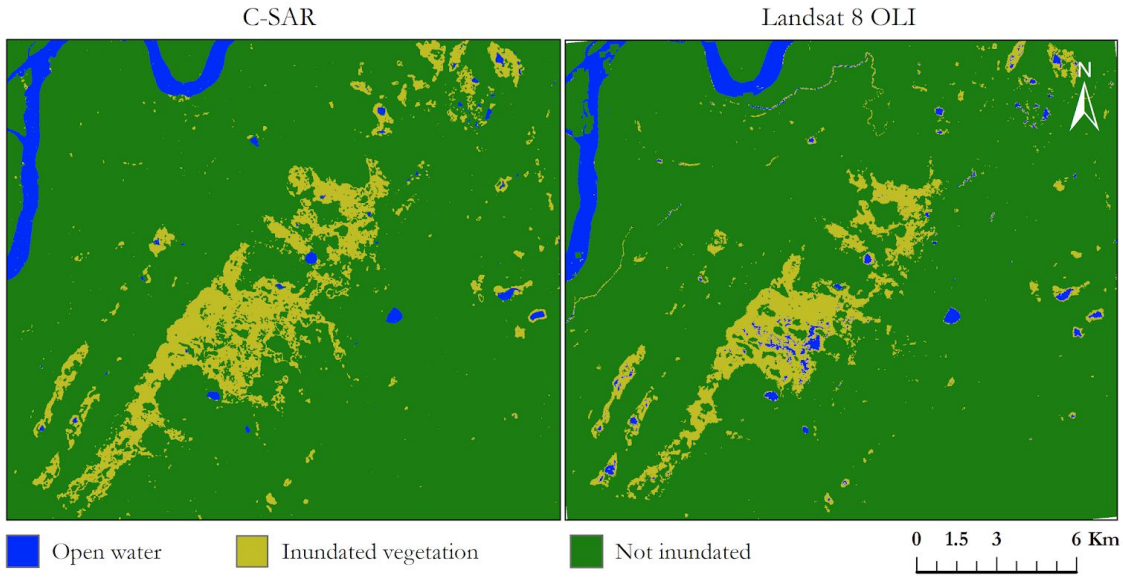

Figure 4. Comparison of the output from the algorithm on C-SAR data and the output of DSWE on Landsat 8 OLI imagery of Bear Lake, Alaska for July 6th, 2017.

To perform an accuracy assessment between the Landsat DSWE and SAR, a confusion matrix was generated using the converted binary classifications (Figure 5). This assessment of the binary classifications prioritizes

the distinction between inundated and non-inundated, as opposed to also examining differences in open water and inundated vegetation.

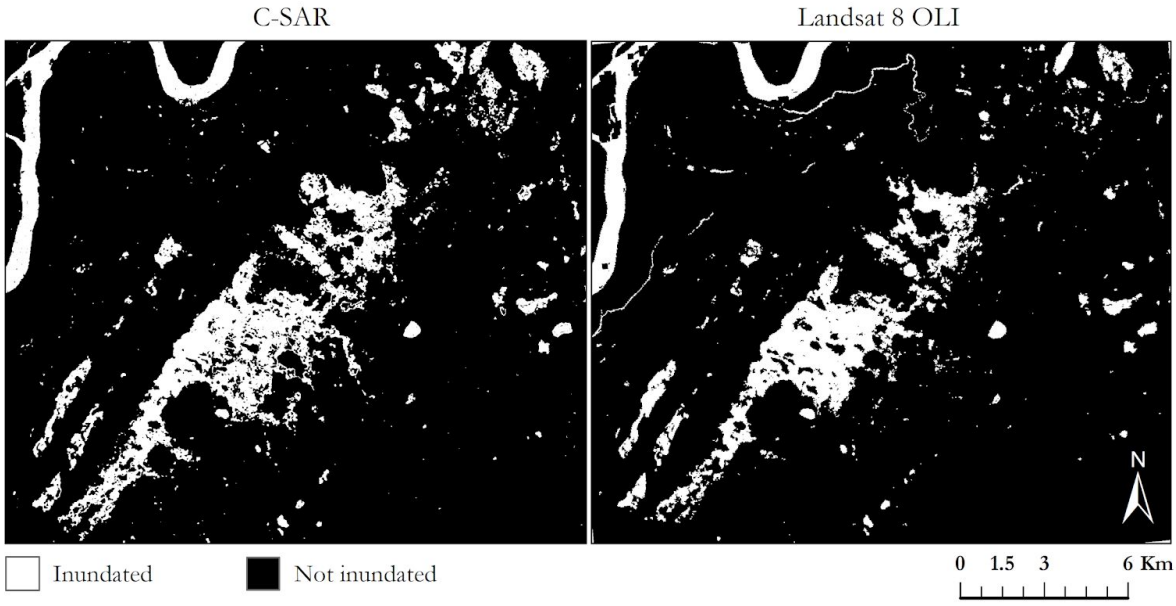

Figure 5. Sentinel-1 C-SAR binary classification July 6, 2017 and Landsat 8 DSWE binary classification July 6, 2017 for Bear Lake, Alaska.

4.1 Analysis of Results

4.1.1 Bear Lake: Main Algorithm Testing Site

When compared to a Landsat DSWE classification for the same date, our C-SAR algorithm output achieved an overall agreement of 94.54% (Table 5). There was a higher agreement between the non-inundated class (95.9%) than between the inundated class (82.8%). The C-SAR classification identified more pixels than the Landsat DSWE as inundated, resulting in a commission error of 31.4%. These pixels tended to be located along the edges of the main region of inundated vegetation in the center of the image. Conversely, inundated pixels that were omitted by our algorithm tended to be located around the edges of the river in the northwestern corner of our image and around the perimeter of smaller bodies of open water throughout the scene. The omission of rivers may due to the multi-look pixel window applied to single-date SAR images to help smooth and reduce speckling. This discrepancy resulted in an omission error of 17.9%.

Table 5

Confusion matrix comparing C-SAR and Landsat 8 DSWE for Bear Lake, Alaska on July 6, 2017.

		Landsat 8 DSWE	
Overall agreement: 94.54%		**Non Inundated**	**Inundated**
C-SAR	**Non Inundated**	95.9%	17.9%
	Inundated	4.1%	82.2%

	Commission	**Omission**

C-SAR	**Non Inundated**	2.0%	4.1%
	Inundated	31.4%	17.9%

4.1.2. Remaining Study Sites

The four other study sites were also classified with our C-SAR algorithm (Figure 6). We determined separate brightness threshold ranges for each site, and the output classifications showed varying degrees of success. We expect that the difference in environmental conditions and hydroperiod at these sites, compared to our main site Bear Lake, resulted in errors when classifying.

Specifically, our C-SAR algorithm saw difficulties mapping open water and rivers on two of our study sites, Canvasback Lake and Crea Creek. Canvasback Lake saw one of our lowest agreements between inundated areas with only 40 percent of these areas coinciding (Table A1). Another of our study sites, Goldstream Valley, in turn saw a very small regions of its area classified as having any degree of inundation. This may be due in part to the site's homogeneous landscape, existing tree canopy covering underlying inundation, or water bodies being too small or slim to be effectively detected and mapped. In Selawik, another one of our study sites, we observed a lot of transition spaces between open water and non-inundated areas. These areas of high variability can often prove challenging to validate between C-SAR and optical data when observation dates are non-coinciding. Although we attempted to find dates that were as close together as possible, that was not always possible with the differing temporal resolutions of both earth observations and cloud cover limiting available optical data. Even in relatively short gaps of data coverage, inundation extent can fluctuate significantly, as highlighted in the difference between outputs of minimum and maximum inundation extent.

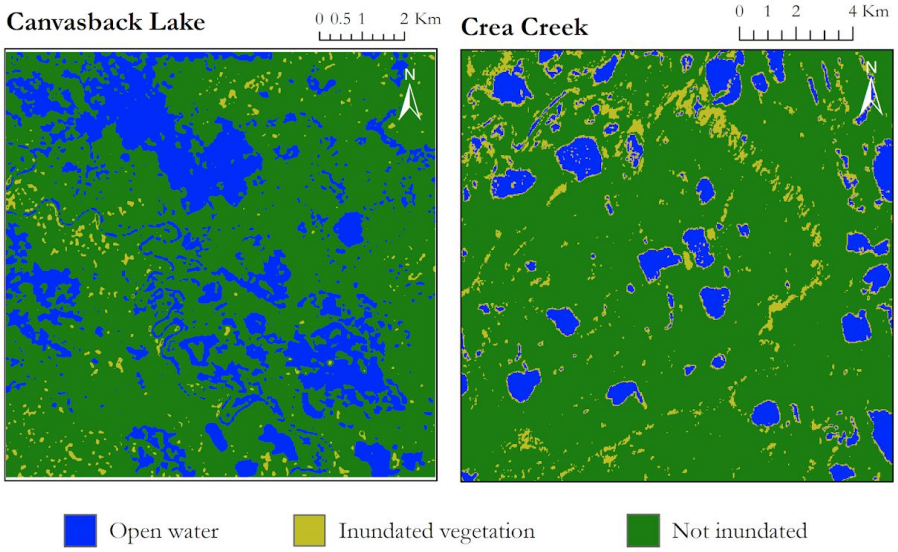

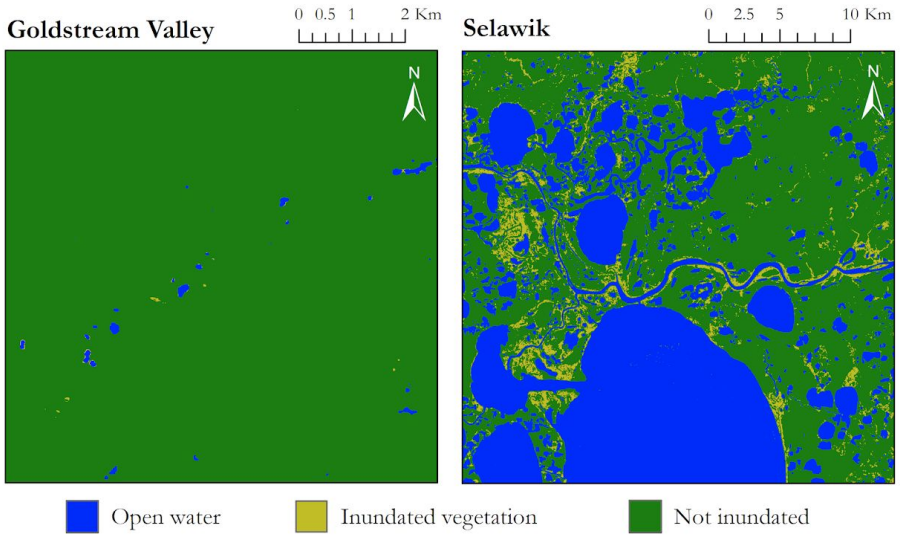

Figure 6. Typical inundation states for Canvasback Lake, Crea Creek, Goldstream Valley, and Selawik derived from C-SAR algorithm for the summer of 2017.

The multi-temporal average classifications or the typical inundation outputs generally matched Landsat DSWE outputs more closely than single-date classifications (Figure 6, Figure A2). This may be due to uncorrected calibration errors and high variations in brightness throughout different dates in the summer of 2017 across these other four sites. Providing more comprehensive and flexible thresholds for our algorithm when performing classifications will allow us overcome some of the limited results from these sites. This will require further calibration, validation and testing. Future availability of in situ data might also allow us to have greater confidence in our outputs even when these might not intuitively appear to be precise.

4.2 Future Work

A second term is proposed for this project with the main goals of further calibration and validation of the algorithm. The team will hopefully incorporate additional datasets such as UAVSAR and ground truth data to improve algorithm thresholds. Since the current state of our algorithm requires manual adjustment by the user, an additional goal is to automate the threshold selection process. While this manual threshold input provides some flexibility for the user, it can be time intensive and does not align with our long term goal of automating the mapping process. Future work could use vegetation cover data to inform differences in threshold values between sites. Unsupervised classification techniques such as image segmentation may be possible methods to automate this algorithm.

Future work could also include the classification refinement. Using the difference between individual time steps and the multi-temporal average, refined classifications can reveal areas that are inundated year-round, seasonally, or not inundated. Once this is fine-tuned, it may be possible to model and forecast inundation and wetland extent. Additionally, we currently only check for calibration errors and do not apply corrections. In the future, when calibration issues are detected, images could be normalized by the multi-temporal averaged brightness value (Chapman et al. 2015).

5. Conclusions

Our results suggest that C-SAR is a useful source of data for identifying inundation. The C-SAR image collection was unhindered by cloud and snow, unlike the data acquisition process for Landsat 8 OLI and Planet Labs optical imagery. Despite this disadvantage, optical data proved to be a useful stand-in for in-situ data when calibrating and validating our C-SAR algorithm thresholds. We identified several issues regarding the accuracy of our classifications and other considerations when utilizing C-SAR data. As shown by our accuracy assessments, there was great variation in correspondence between our C-SAR products and DSWE products. This could be attributed to varying water regimes and vegetation type and density at each site. Another factor that may have influenced our product was the improper co-registration of our images. This could have caused small regions of inundation to be lost in the multi-temporal average, leading to omission errors.

Further work needs to be conducted to adjust our algorithm to better resemble classification products generated from optical data. Upon further refinement, this algorithm could enhance the wetland mapping capacity of our partners at the National Wetland Inventory. Additionally, once the robustness of the C-SAR data and thresholds are established, the data can be more confidently used to map areas of inundation that traditional mapping methods and optical imagery are unable to detect, such as below dense canopy cover.

6. Acknowledgments

The Alaska Ecological Forecasting team would like to thank the mentors and partners who provided their support and time to make this project possible, specifically our science advisor Bruce Chapman at JPL, and project partners Dr. Megan Lang at the USFWS and Jeremy Nicoll and Franz Meyer at ASF.

RapidEye and PlanetScope Imagery courtesy of Planet Labs, Inc.

This material contains modified Copernicus Sentinel data (2017), processed by ESA.

Any opinions, findings, and conclusions or recommendations expressed in this material are those of the author(s) and do not necessarily reflect the views of the National Aeronautics and Space Administration.

This material is based upon work supported by NASA through contract NNL16AA05C.

7. Glossary

ASF - Alaska Satellite Facility. Part of the Geophysical Institute of the University of Alaska Fairbanks.
ASF Vertex - Data acquisition portal of the Alaska Satellite Facility for remotely sensed data of the Earth.
Co-registration - Process of accurately aligning the same geographical locations on different data sets. Essential when performing analysis or change detection processes.
Earth Explorer - USGS satellite, aerial imagery, and remote sensing data catalog.
Earth observations - Satellites and sensors that collect information about the Earth's physical, chemical, and biological systems over space and time.
ENVI - Image analysis software and file format which incorporates an image file and a header ASCII file containing the image's metadata and other metrics.

GDAL - Geospatial Data Abstraction Library. Shell and Python script library for processing vector and raster geospatial data.
GeoTIFF - File format which integrates georeferenced geographical data with TIFF imagery.
Hydroperiod - Seasonal pattern of water levels. Wetlands may display tidal, permanent, intermittent, seasonal, or even just temporary flooding
HyP3 - Hybrid Pluggable Processing Pipeline. Tool for providing on demand processed Sentinel radar data.
NWI - National Wetlands Inventory. Established by the US Fish and Wildlife Service.
SAR - Synthetic Aperture Radar. Radar system which utilizes the flight path of the space or airborne platform to simulate very large antenna. Capable of generating high-resolution radar imagery.
USFW - United States Fish and Wildlife Service
VV - vertical transmit, vertical receive. Radar system wave polarization consisting of vertical linear transmission and vertical linear reception
VH - vertical transmit, horizontal receive. Radar system wave polarization consisting of vertical linear transmission and horizontal linear reception

8. References

Brooks, R. T. (2000). Annual and seasonal variation and the effects of hydroperiod on benthic macroinvertebrates of seasonal forest ("vernal") ponds in central Massachusetts, USA. *Wetlands*, *20*(4), 707.

Chapman, B., McDonald, K., Shimada, M., Rosenqvist, A., Schroeder, R., Hess, L. (2015). Mapping regional inundation with spaceborne L-band SAR. *Remote Sensing*, *7*(5), 5440–5470. https://doi.org/10.3390/rs70505440

Hall, J. V., Frayer, W. E., & Wilen, B.O. (1994). Status of Alaska Wetlands, 36.

Hogenson, K., Arko, S.A., Buechler, B., Hogenson, R., Herrmann, J. & Geiger, A. (2016). Hybrid Pluggable Processing Pipeline (HyP3): A cloud-based infrastructure for generic processing of SAR data. Abstract [IN21B-1740] presented at 2016 AGU Fall Meeting, San Francisco, CA, 12-16 December.

Jones, J. W. (2015). Efficient wetland surface water detection and monitoring via Landsat: Comparison with in situ data from the Everglades Depth Estimation Network. Remote Sensing, 7(9), 12503-12538. http://dx.doi.org/10.3390/rs70912503

Kasischke, E. S., Melack, J. M., & Craig Dobson, M. (1997). The use of imaging radars for ecological applications—A review. *Remote Sensing of Environment*, *59*(2), 141–156. https://doi.org/10.1016/S0034-4257(96)00148-4

Lang, M. W., Kasischke, E. S., Prince, S. D., & Pittmn, K. W. (2008). Assessment of C-band synthetic aperture radar data for mapping and monitoring Coastal Plain forested wetlands in the Mid-Atlantic Region, U.S.A. *Remote Sensing of Environment*, *112*(11), 4120–4130. https://doi.org/10.1016/j.rse.2007.08.026

Tiner, R. (1990). Use of high-altitude aerial photography for inventorying forested wetlands in the United States. *Forest Ecology and Management*, *33 – 34*, 593–604. https://doi.org/10.1016/0378-1127(90)90221-V

Townsend, P. A. (2002). Relationships between forest structure and detection of flood inundation in forested wetlands using C-band SAR. *International Journal of Remote Sensing*, 67, 857-864. https://doi.org/10.1080/01431160010014738

Tsyganskaya, V., Martinis, S., Marzahn, P., & Ludwig, R. (2018). SAR-based detection of flooded vegetation – a review of characteristics and approaches. *International Journal of Remote Sensing, 39*(8), 2255–2293. https://doi.org/10.1080/01431161.2017.1420938

US Fish and Wildlife Service. (2018). NWI Program Overview. Retrieved October 1, 2018. https://www.fws.gov/wetlands/nwi/overview.html

US Geological Survey Earth Resources Observation and Science Center. (2017). Landsat 8 OLI/TIRS Level-2 Data Products – Surface Reflectance. [Image collection]. US Geological Survey, accessed 3 Oct 2018. https://doi.org/10.5066/F78S4MZJ.

Wilen, B.O., & Bates, M.K. (1995). The US Fish and Wildlife Service's National Wetlands Inventory Project. *Vegetatio* 118, 153-169. https://doi.org/10.1007/BF00045197

9. Appendix

Table A1

Location, and NWI wetland classification type of study sites (National Wetlands Mapper).

Site	Location	Wetland Type
Crea Creek	70.2, -152.5	Lakes/Ponds Freshwater Emergent Wetland
Yukon Flats (Canvasback Lake)	66.389, -146.363	Lake with Freshwater Forested/Shrub and Emergent Wetland
Bear Lake	64.734, -149.737	Freshwater Emergent Wetland
Selawik	66.525, -159.097	Active Mapping
Goldstream	64.8944, -147.8719	Freshwater Forested/Shrub Emergent Wetland
Area 1002	70.0474, -143.2261	Active Mapping

Figure A1:

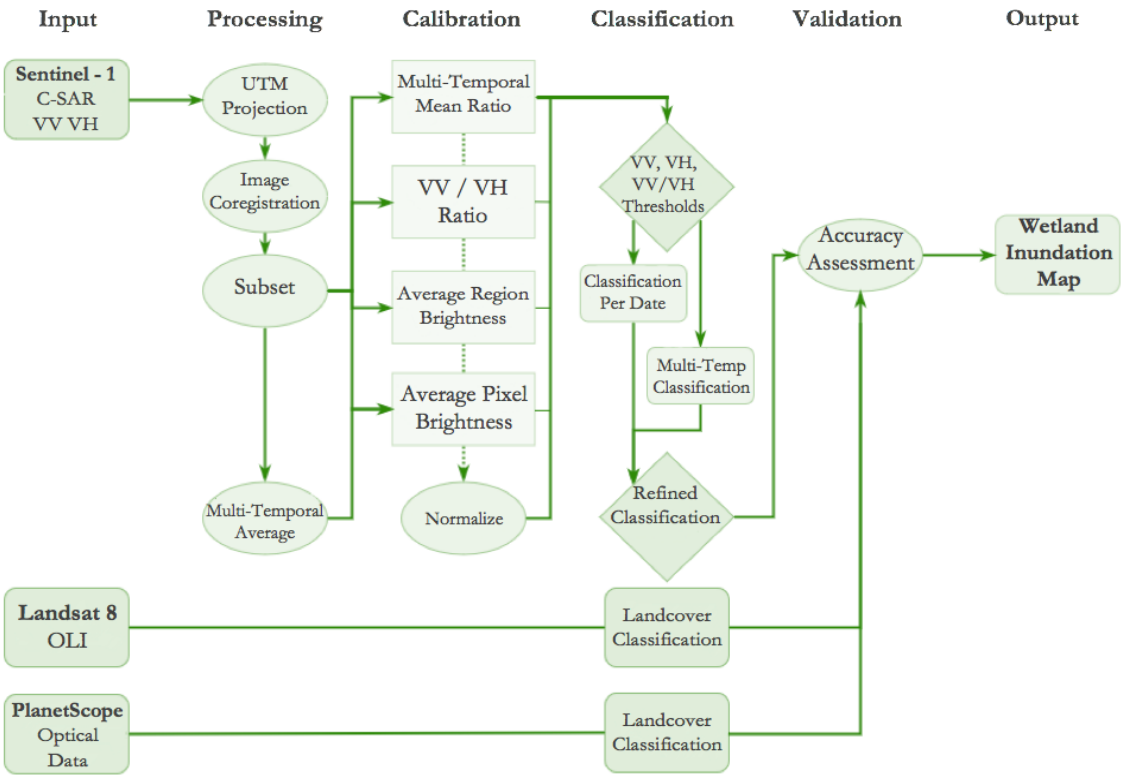
Input
Processing
Calibration
Classification
Validation
Output
Sentinel - 1
C-SAR
VV VH
UTM
Projection
Image
Coregistration
Subset
Multi-Temporal
Average
Multi-Temporal
Mean Ratio
VV / VH
Ratio
Average Region
Brightness
Average Pixel
Brightness
Normalize
VV, VH,
VV/VH
Thresholds
Classification
Per Date
Multi-Temp
Classification
Refined
Classification
Accuracy
Assessment
Wetland
Inundation
Map
Landsat 8
OLI
Landcover
Classification
PlanetScope
Optical
Data
Landcover
Classification

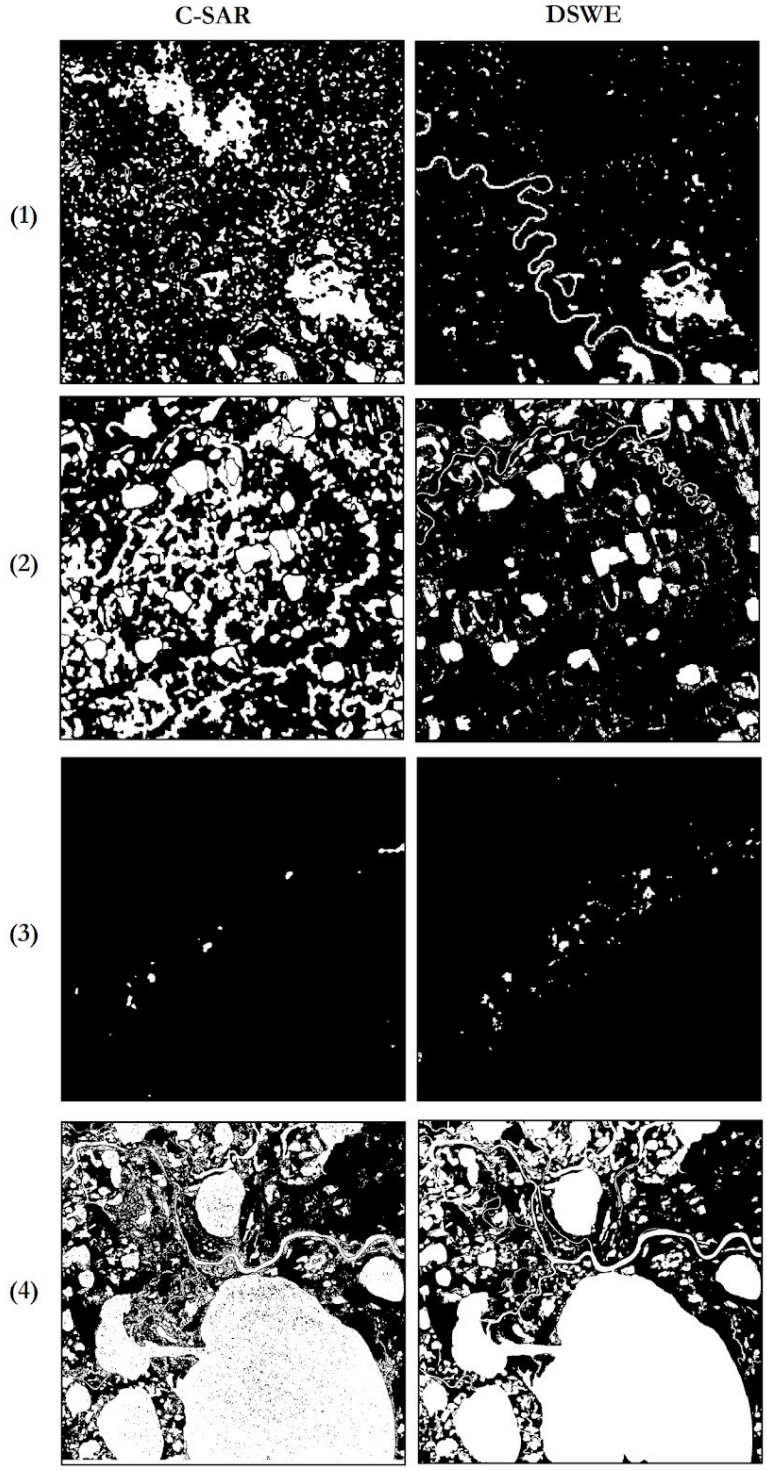

Figure A2. Comparisons of C-SAR algorithm classification and Landsat 8 DSWE classification for (1) Canvasback Lake, (2) Crea Creek, (3) Goldstream Valley and (4) Selawik. Black regions are non-inundated and white regions are inundated.

Table A2

Confusion matrix comparing C-SAR and Landsat 8 DSWE for Canvasback Lake, Alaska.

		Landsat 8 DSWE - 6/4/17	
Overall agreement: 94.54%		**Non Inundated**	**Inundated**
C-SAR 6/12/17	**Non Inundated**	96.77%	59.77%
	Inundated	3.23%	40.23%

		Commission	**Omission**
C-SAR 6/12/17	**Non Inundated**	2.0%	4.1%
	Inundated	31.4%	17.9%

Table A3

Confusion matrix comparing C-SAR and Landsat 8 DSWE for Crea Creek, Alaska.

		Landsat 8 DSWE - 7/9/17	
Overall agreement: 94.54%		**Non Inundated**	**Inundated**
C-SAR 7/4/17	**Non Inundated**	92.4%	31.4%
	Inundated	7.66%	68.6%

		Commission	**Omission**
C-SAR 7/4/17	**Non Inundated**	5.3%	7.6%
	Inundated	40.6%	31.4%

Table A4

Confusion matrix comparing C-SAR and Landsat 8 DSWE for Goldstream Valley, Alaska.

		Landsat 8 DSWE - 6/13/17	
Overall agreement: 99.78%		**Non Inundated**	**Inundated**
C-SAR 6/12/17	**Non Inundated**	99.7%	77.4%
	Inundated	0.04%	22.6%

		Commission	**Omission**
C-SAR 6/12/17	**Non Inundated**	0.2%	0.04%
	Inundated	41.7%	77.42%

Table A5

Confusion matrix comparing C-SAR and Landsat 8 DSWE for Selawik, Alaska.

Overall agreement: 94.54%		Landsat 8 DSWE - 7/21/17	
		Non Inundated	**Inundated**
C-SAR 7/16/17	**Non Inundated**	93.2%	24.9%
	Inundated	6.7%	75.1%

		Commission	**Omission**
C-SAR 7/16/17	**Non Inundated**	24.7%	6.7%
	Inundated	6.8%	24.9%